PROCEEDINGS of the
23rd International Congress on Acoustics

9 to 13 September 2019 in Aachen, Germany

# Influence of the Mesh Size on the Aerodynamic and Aeroacoustics of a Centrifugal Fan using the Lattice-Boltzmann Method

Rebecca SCHAEFER[1]; Martin BOEHLE[2]

[1] University of Kaiserslautern, Germany

[2] University of Kaiserslautern, Germany

## ABSTRACT

The present paper deals with the direct and coupled simulation of the aerodynamics and aeroacoustics of a centrifugal fan connected to a suction-side test bench using the commercial Lattice-Boltzmann Code PowerFLOW of the Exa Corporation. The focus is on the variation of the mesh size in the finest grid resolution, which influence the time step immensely. The aim is to determine the smallest grid size in such a way that both the flow and acoustics of the centrifugal fan can be accurately predicted with an acceptable total computing time. In this study, three different mesh sizes for two different geometries of the finest resolution area will be investigated and compared.

The results of the Lattice-Boltzmann simulation are compared and validated with measurement results obtained according to an ISO standard procedure at the Institute of Fluid Mechanics and Fluid Machinery at the University of Kaiserslautern. Flow information in term of the pressure increase of the centrifugal fan is well captured by the simulation. In addition, the noise is well predicted with respect to blade passing frequency and the general level of the spectrum at the considered microphone positions.

Keywords: Lattice-Boltzmann Method, Centrifugal Fan, Aeroacoustics

## 1. INTRODUCTION

Due to market requirements and ever stricter guidelines, noise emissions of fans are becoming increasingly important in addition to energy efficiency. This applies in particular when people have to work near running fans. For this reason, the development of fans aims not only at more efficient running fans but also ever quieter fans. In order to keep the development process cost-effective and as short as possible, numerical investigations are used today. Classic numerical methods do not allow to calculate aerodynamics coupled with aeroacoustics. The Lattice- Boltzmann method is a relatively new method that promises to close this gap. It always solves for the unsteady flow field using relatively small time steps which allow for an accurate resolution of the alternating pressures that are responsible for the acoustics. This allows to solve the sound pressures directly without using an acoustic model. Also, the method is known to be low dissipative, which could be shown by Marié et al. (1). Therefore, the LBM is ideally suited for the simulation of aeroacoustics. A big advantage of the Lattice-Boltzmann method is also that it is more or less an immersed boundary method. Flow areas of complex geometry can be meshed without effortful geometry preparation, which leads to a huge time saving.

Perot et al. (2) could show that the LBM can be used to determine the performance and frequency spectrum of an axial fan. Also Zhu et al. (3) and Sturm et al. (4) could successfully show that the aerodynamics and aeroacoustics for an axial fan with different head gaps and under different inflow conditions can be calculated with the commercial LBM code PowerFLOW of the company Exa. There are also some studies on centrifugal fans where the performance and acoustics have been successfully calculated using PowerFLOW. The fans were connected on the pressure-side and the investigation of the influence of so-called obstructions was in focus. (5, 6)

In this paper, the commercial Lattice-Boltzmann code PowerFLOW is used to simulate the flow and acoustics in a centrifugal fan without a volute casing connected to a suction-side test bench. A detailed mesh study is in focus. Two different geometries are selected for refinement because it has

[1] Rebecca.schaefer@mv.uni-kl.de
[2] Martin.boehle@mv.uni-kl.de

been shown that the choice of the refinement zone has an immense influence on the results especially regarding the acoustics. In the first case an offset of the impeller geometry is chosen for refinement, in the second case an addition donut-like ring in areas of high velocity is selected to set a finer resolution.

For the validation of the LBM simulation, aerodynamic and aeroacoustics measurements are performed on the institute's own fan test bench, which was developed according to DIN ISO 5801. The results of the LBM simulation are compared to the experimental results.

## 2. FUNDAMENTALS OF THE LATTICE-BOLTZMANN METHOD

### 2.1 Velocity Distribution Function

In contrast to the Navier-Stokes equation, which is based on a macroscopic view, the Lattice-Boltzmann Method uses a mesoscopic approach. A molecular consideration is taken in which the molecular movements are described statistically. The molecules themselves are characterized by a so called velocity distribution function, which is given in Equation (1).

$$f(x,\xi,t) = \frac{dN}{dV \cdot d\xi} \tag{1}$$

It describes the probability of finding dN molecules with a certain velocity dξ at a certain point in space dV.

### 2.2 Boltzmann-Equation

The Boltzmann equation is a generally valid determination equation for the distribution function f. Due to the fact that it is a complex integro-differential equation, it cannot be solved even with modern methods. The derivation of the Boltzmann equation is based on the preservation of the particles in the phase space. The basis form in tensor notation is presented as

$$\frac{\partial f}{\partial t} + \xi_i \cdot \frac{\partial f}{\partial x_i} + \frac{F_i}{m} \cdot \frac{\partial f}{\partial \xi_i} = \Omega_K(f) \tag{2}$$

where f = f (x,ξ,t) is the above described velocity distribution function. The left side of Equation (2) contains the time and convective change of the distribution function as well as the change due to external forces $F_i$. The right side of Equation (2) describes the change of the distribution function due to interaction of the particles and is called the collision term. Since the collision term is composed of a complex integral, it is approximated by a much simpler mathematical approach. Often the so-called BGK model according to Bhatnagar, Gross and Krook (7) is used. This assumes that every non-equilibrium condition leads to an equilibrium condition, cf. Equation (3)

$$\Omega_K(f) = -\omega \cdot (f - f^{eq}) \tag{3}$$

ω describes the molecular collision frequency and indicates the number of transitions from non-equilibrium to equilibrium per time interval t. f stands for the non-equilibrium distribution and $f_{eq}$ for the local equilibrium distribution. The equilibrium distribution is equal to the Maxwell distribution. (8, 9) Using the BGK model (7) for the collision modeling and a Chapman-Enskog development (8) the Boltzmann Equation in Equation (2) recovers the Navier-Stokes equation.

### 2.3 Lattice-BGK-Equation

In order to solve the BGK-Boltzmann equation numerically, a discretization in time and phase space has to be applied. In the latter case, a spatial discretization of the Cartesian space into an equidistant mesh is performed, cf. Figure1. Each mesh cell is called a lattice.

In addition to the spatial discretization, the velocity is discretized to predefined velocity directions. In the three-dimensional case, model D3Q19 is often used. This is also implemented in PowerFLOW. The model works with i = 19 defined directions, which are indicated by $\xi_i$ in Figure 1.

The discrete BGK-Boltzmann equation presented in Equation (4) is called the Lattice-BGK or the LBGK equation.

$$f_i(x + \xi_i \cdot \partial t, t + \partial t) = f_i(x,t) + \omega \cdot \partial t \cdot \left(f_i^{eq}(x,t) - f_i(x,t)\right) \tag{4}$$

The equation indicates that a calculation step consists of a transport step $f_i(x,t)$ and a collision step $\omega \cdot \partial t \cdot f_i^{eq}(x,t) - f_i(x,t)$. Algorithmically, these two steps are usually calculated separately for

each velocity $\xi_i$ in each lattice per time step. In an explicit procedure the new distribution functions $f_i(x,t)$ for the next time step $t + \partial t$ can be determined.

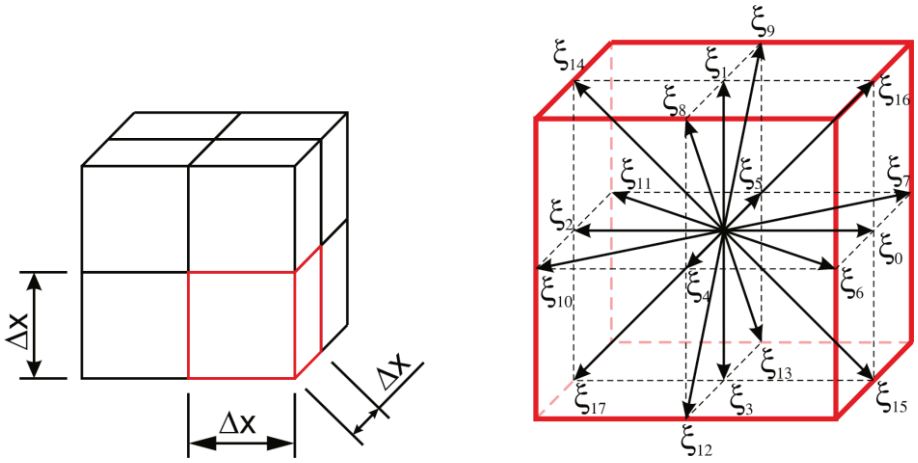


Figure 1 – Spatial discretization (left) and model of D3Q19 of the velocity discretization (right)

With the known distribution function f (x,ξ,t) the macroscopic quantities of interest can be calculated by determining the so-called moments. It is shown in Equation (5) and (6) exemplary for the calculation of macroscopic density and velocity.

$$\rho(x,t) = \sum_{i=1}^{q-1} f_i(x,t) \tag{5}$$

$$\rho \cdot u(x,t) = \sum_{i=1}^{q-1} \xi_i \cdot f_i(x,t) \tag{6}$$

### 2.4 Selection of Timestep

The timestep selection is based on the fact that a particle moves with the velocity $\xi_0$ in one timestep exactly one lattice length Δx. The particle velocity $\xi_0 = \sqrt{3} \cdot c_s$ is determined by the so-called simulation Mach number $Ma_{sim} = {}^{c_{char}}/_{c_s}$ with the characteristic velocity $c_{char}$ and the isothermal speed of sound $c_s$. The timestep Δt can thus be determined from

$$\Delta t = Ma_{sim} \cdot \frac{1}{\sqrt{3}} \cdot \frac{\Delta x}{c_{char}} \tag{7}$$

whereby the simulation Mach number $Ma_{sim}$ in only a scaling factor with which ensures that the characteristic velocity $c_{char}$ is one scale order smaller than the speed of sound. (8) In the case of acoustic problems, the simulation Mach number $Ma_{sim}$ is set equal to the physical Mach number $Ma_{real} = {}^{u}/_{a_s}$, so that the time step is ultimately only dependent on the grid size Δx.

## 3. EXPERIMANTAL SETUP

### 3.1 Test Rig

The experimental investigations were performed on the fan test rig in the anechoic room of the Institute of Fluid Mechanics and Fluid Machinery of the University of Kaiserslautern. It is a suction-side chamber test bench, which is developed according to DIN EN ISO 5801 and is schematically shown in Figure 2.

The test bench consists of two main components: the inlet section and the suction chamber. The inlet section includes an inlet nozzle, a diffusor, a throttle and a pipe section. All components of the inlet section with the exceptions of the pipe section, which connects the inlet section with the suction chamber, are located outside the anechoic room. This should ensure that the noise, which is generated by the throttle, is decoupled to the acoustic measurements of the fan. In addition, perforated discs according DIN EN ISO 5136 are used, which allow low-noise throttling due to the uniform distribution

of the holes. The inlet nozzle, at which the differential pressure $\Delta p_0$ is measured, is used to determine the volume flow. The differential pressure $\Delta p_1$ is acquired to determine the pressure increase of the fan. Furthermore, the temperature and the ambient pressure in the anechoic room, which are used for the physical conditions in the simulation, are recorded. The sound pressure is measured on a hemisphere behind the fan connected to the suction chamber. As in the simulation, the sound pressure and aerodynamic parameters are measured simultaneously.

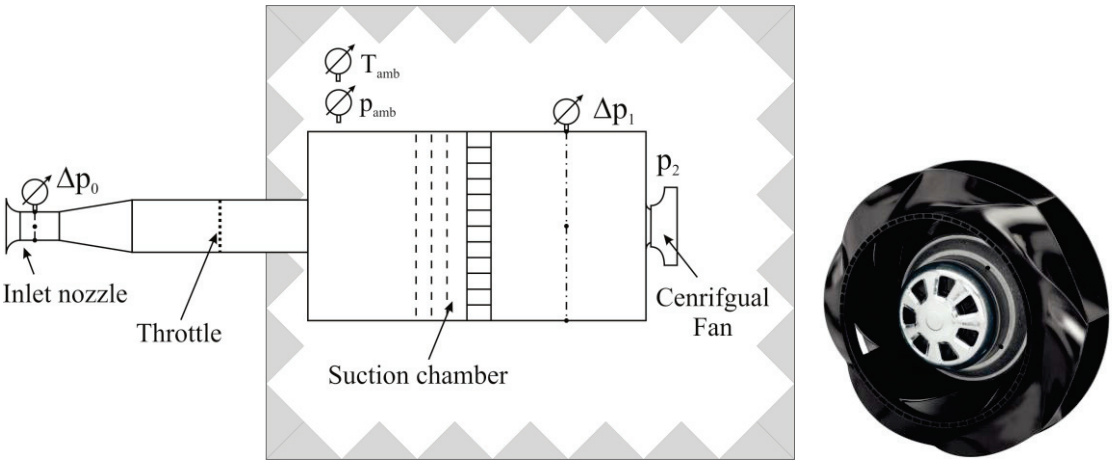


Figure 2 – Schematic of the fan test rig (left) and investigated centrifugal fan (cf. (10)) (right)

### 3.2 Measurement Technique

The aerodynamic of a fan is quantified by the pressure increase and the efficiency. The values are calculated according to DIN EN ISO 5801. In Equation (8) the formula for the static pressure increase of the fan is given. The indices 1 and 2 indicate the position of the evaluation position upstream and downstream of the fan, whereby the ambient pressure $p_{amb}$ is be assumed for the pressure $p_{st2}$.

$$\Delta p_{fa} = p_{st2} - \left(p_{st1} + \frac{\rho}{2} \cdot c_1^2\right) \tag{8}$$

The aeroacoustics of a fan is determined by the sound pressure level $L_p$ as well the total sound pressure $\bar{L}_p$ obtained from the frequency analysis. The quantities are defined according DIN 45635-1 and are given in Equation (9) and (10) with p as the alternating pressures and $p_0$ as the reference sound pressure level.

$$L_p = 20 \cdot log\left(\frac{p}{p_0}\right) dB \tag{9}$$

$$\overline{L_p} = 10 \cdot log \sum_{i=1}^{n} 10^{0.1 \cdot L_{pi}} \tag{10}$$

## 4. NUMERICAL SETUP AND PARAMETER

The commercial LBM-Code PowerFLOW 6-2019 is used to compute the unsteady flow field and the acoustic of a centrifugal fan without the volute casing. Because the pressure loss of the screens and the honeycomb inside the suction chamber are not known until now the simulation area starts at the pressure measurement location $\Delta p_1$, cf. Figure 2 and 3. The overall simulation area includes the anechoic room; foams at the walls are modelled with so-called sponge zones, where the viscosity is increased over three layers. A velocity boundary is selected as the inlet boundary condition. The velocity corresponds to the mean velocity resulting from the measured volumetric flow. At the boundaries of the overall simulation area a pressure outlet is set. The rotation of the fan is modelled by a local reference frame (LRF) with the sliding mesh approach using the rotating speed obtained by the measurements.

Several variable resolution (VR) regions are used to refine the computational domain, some of them are shown in grey in Figure 3. Two different studies of the geometry for the finest resolution are compared: In the first case the refinement for the grid study is done by an offset of the impeller

geometry. The offset is chosen so that the gap between the impeller and the impeller inlet nozzle is also refined and the flow can be dissolved. In the following, this method is referred to as “Offset” refinement.

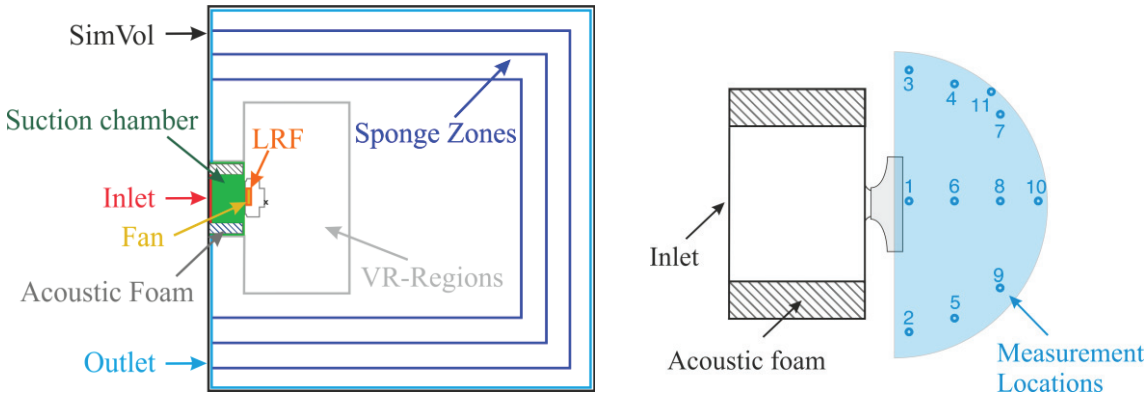


Figure 3 – Simulation model (left) and measurement locations (right)

In the second case the refinement is done by a ring which resolves the high velocity regions at the impeller’s outlet and the gap between the impeller and the impeller inlet nozzle. In the ensuing, this case is named as “Donut” refinement. Three different meshes will be studied for the two different refinement cases - one fine mesh with finest cell size of $\Delta x$ =0.2 mm, one medium with $\Delta x$ = 0.4 mm and one coarse with $\Delta x$ =0.8 mm.

In Figure 3 the positions of the microphone locations are shown on the right side. The grid resolution of $\Delta x_5$ = 12.8mm is determined in the area of the microphone positions. According to Brès (11) et al., at least 12 – 16 grid points per wavelength should be selected for the propagation of sound waves, which results to a maximum cutoff frequency of around $f_{max}$ = 1.7 kHz – 2.2kHz.

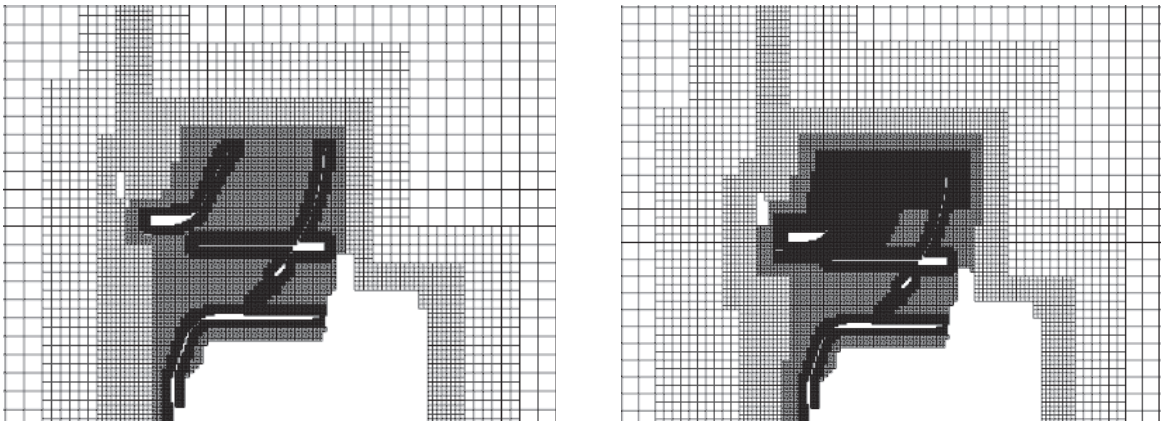

Figure 4 – Mesh with offset refinement (left) and with donut refinement (right)

In Figure 4 a section of the discretization of the computational domain in a cross-sectional area through the impeller main axis for the two different refinement cases representative with the medium mesh are shown. In Table 1 the total number of voxel of the different meshes is presented.

For the simulation Mach number, the real physical Mach number is used, which leads to a Mach number of approximately $Ma_{sim}$ = 0.1.

Table 1 – Total number of voxels of the different meshes

| Mesh size | Offset Refinement | Donut Refinement |
|---|---|---|
| Coarse (0.8 mm) | 26.6 x $10^6$ | 9.7 x $10^6$ |
| Medium (0.4 mm) | 35.0 x $10^6$ | 31.3 x $10^6$ |
| Fine (0.2 mm) | 106.1 x $10^6$ | 183.7 x $10^6$ |

The simulation is executed over a physical time of approximately 0.85 s. Convergence is archived

after approximately 0.2 s physical time, which corresponds to approximately 12.0 impeller revolutions. The evaluations are made over a signal time of 0.65 s. The simulations are performed on Intel XEON E5-2670 processors in case of the offset refinement and on Intel XEON SP 6126 in case of the donut refinement. In Table 2 the CPU-h per impeller revolution are listed for the different meshes.

Table 2 – CPU-h per impeller Revolution for the different meshes

| Mesh size | Offset Refinement | Donut Refinement |
|---|---|---|
| Coarse (0.8 mm) | 99.2 | 71.3 |
| Medium (0.4 mm) | 291.4 | 298.4 |
| Fine (0.2 mm) | 2103.6 | 2642.1 |

## 5. RESULTS

In order to make the results comparable to the measurements, the same settings for the evaluation of the power spectrum are used for simulation and measurement, cf. Table 3.

Table 3 – Settings for evaluation of the power spectrum

| Parameter | Settings |
|---|---|
| Frequency resolution | 6.25 Hz |
| Window | Hanning |
| Signal length | 0.65 s |
| Window overlapping | 50 % |
| Averaging | linear |

In Figure 5 on the left side the fan's pressure increase is presented over the different mesh sizes for the two refinement approaches "Offset" and "Donut". In both approaches the simulation results converges to the experimental values with finer mesh. The deviation between the fine mesh and the medium mesh as well between the two refinement approaches are very small, but better results are obtained by the donut refinement. With that refinement case and the fine mesh an absolute deviation of approximate 8 Pa is achieved which correspond to a relative deviation of 2 %. The greatest deviation is around 10 % with the coarse mesh.

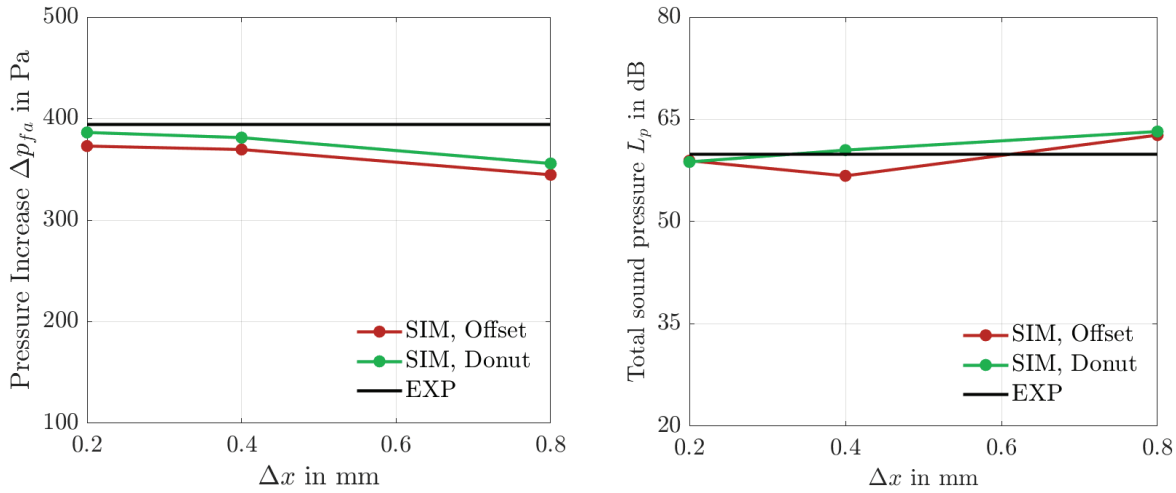


Figure 5 – Pressure increase (left) and total sound pressure (right) over the mesh size

The total sound pressure level is also shown in Figure 5 on the right side. Here, the choice of refinement geometry has a greater influence on the results. Best results are received by the fine and medium mesh with the donut refinement where the relative deviation is around 1 - 2 %. The deviations of the offset refinement are up to 6 % compared to the experiment.

To better understand where the deviations are exactly, the sound pressure above the frequency is shown in Figure 6. On the left side the power spectrum of the offset refinement is presented and on the right of the donut refinement. Areas above the cutoff frequency, which results from the grid resolution in the area of the microphone positions, are marked in grey. Also the blade passing frequencies (BPF) is marked as grey dotted line.

In both cases, the coarse mesh does not reproduce the acoustics of the fan well. A similar shape as with the coarse mesh can also be achieved with the medium mesh with offset refinement (cf. Figure 6, left). There is a drop of the spectrum noticeable starting at approximately 800 Hz with those three meshes. This indicates that the flow in high velocity regions, which is discretized with 0.8 mm cells, is not completely resolved. No cutoff frequency in the range of 800 Hz is detectable with the fine mesh and the medium mesh with donut refinement, which seems that a cell size of 0.4 mm is sufficient to resolve the high velocity areas.

With all meshes except the fine mesh with offset refinement, the blade passing frequency is captured very well. The best agreement can be obtained by the medium mesh. The coarse mesh slightly overestimates the amplitude of the blade passing frequency and with the fine mesh it is slightly underestimated. So in total, the results show that a simple offset refinement is not sufficient to depict the acoustics correctly.

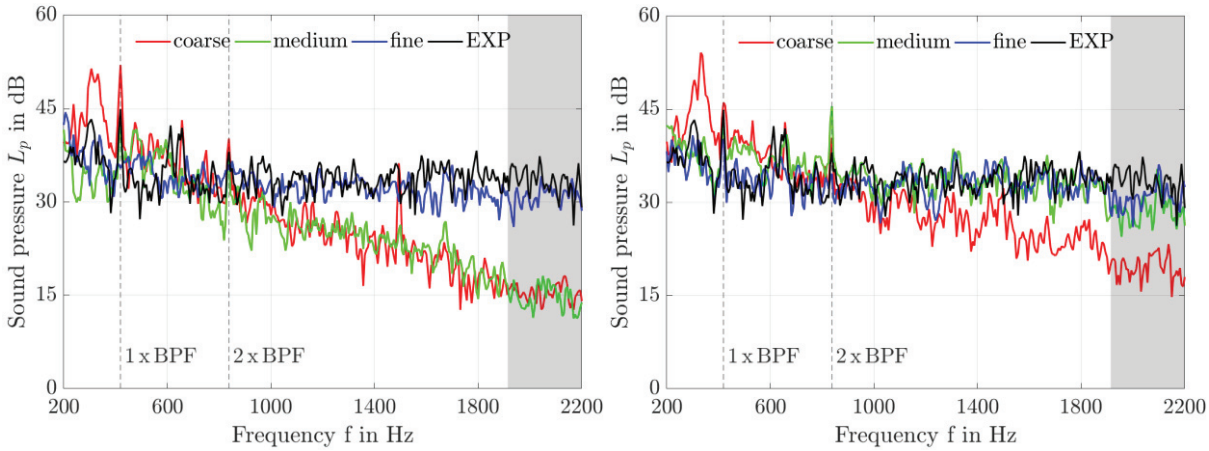


Figure 6 – FFT of offset refinement (left) and donut refinement (right) with different mesh sizes

If the accuracy of the simulation results is considered together with the computation time, which is given in Table 2, it turns out that the best compromise between accuracy and computation time is available with the medium mesh and the donut refinement. The flow in the form of the pressure increase of the fan is still represented with an accuracy of 3 % and the acoustics in the form of the total sound level with approximately 2 % deviation in comparison to the experiment. The blade passing frequency and the general sound power level except in the range of 500 Hz and 800 Hz are very well achieved. It is assumed that the overestimation can be explained by the fact that the boundary layer of the impeller surface with 0.4 mm is not as well resolved as with 0.2 mm. However, this needs further investigations.

## 6. CONCLUSION AND OUTLOOK

In this paper a direct and coupled simulation of the aerodynamic and aeroacoustics of a centrifugal fan with the commercial Lattice-Boltzmann Code PowerFLOW was executed. A mesh size study, where the finest cell size was varied, was performed. Two different geometries to set the finest cell size was analyzed and compared. It could be shown that the shape of the refinement geometry has an influence on the results, especially on the acoustics. A simple offset of the impeller geometry is not sufficient for the refinement to reproduce the acoustics by the simulation, but improvements in performance can be observed. Very good results can be achieved if, in addition, a refinement in the form of a donut-like ring geometry in the range of high velocity areas is taken into account. Best result regarding accuracy and computational effort can be obtained with a medium mesh with a cell size of 0.4 mm with the donut-like ring refinement.

In future investigation additional centrifugal fan's operating points could be analyzed and the case setup could be extended to include also the volute casing. In addition, geometry changes can be made

to the volute casing in order to determine whether these can also be reproduced with the Lattice-Boltzmann simulation. In addition to these points, the simulation and the measurement are compared under visual aspects in order to gain a deeper understanding of the noise generation mechanisms.

## ACKNOWLEDGEMENTS

The study was funded by the German Federal Ministry of Economics and Energy (BMWi) via the "Arbeitsgemeinschaft industrieller Forschungsvereinigungen Otto von Guericke e.V." (AiF) and the "Forschungsvereinigung für Luft und Trocknungstechnik e.V." (FLT). The numerical simulations were executed on the high performance cluster "Elwetritsch", which is part of the "Alliance of High Performance Computing Rhineland-Palatinate" (AHRP) and is managed by the regional computer center of the University of Kaiserslautern (RHRK).

## NOMENCLATURE

| **Symbols** | | **Subscripts and Greek Symbols** | |
|---|---|---|---|
| c | Velocity | 1 | Inflow |
| f | Frequency | 2 | Outflow |
| f | Velocity distribution function | amb | Ambient |
| $L_p$ | Sound pressure | char | Characteristic |
| Ma | MACH Number | eq | Equilibrium |
| p | Pressure | fa | Free blowing |
| $p_o$ | Reference sound pressure level | $\Delta x$ | Lattice size |
| Q | Volume flow | $\rho$ | Density |
| t | Time | $\xi$ | Velocity of particles |
| u | Circumferential velocity | $\omega$ | Collision frequency |

## REFERENCES

1. Marié S, Ricot D, Sagaut P. Comparison between lattice Boltzmann method and Navier–Stokes high order schemes for computational aeroacoustics. Journal of Computational Physics 2009; 228(4):1056–70.
2. Perot F, Moreau S, Kim M-S, Henner M, Neal D. Direct aeroacoustics predictions of a low speed axial fan. In: 16th AIAA/CEAS Aeroacoustics Conference. Stockholm, Sweden, June 07-09, 2010.
3. Zhu T, Sturm M, H Carolus T, Neuhierl B, Perot F. Experimental and numerical investigation of tip clearance noise of an axial fan using a Lattice Boltzmann Method. In: 21st International Congress on Sound and Vibration 2014 (ICSV 21). Beijing, China, July 13-17, 2014.
4. Sturm M, Sanjose M, Moreau S, Carolus T. Aeroacoustic simulation of an axial fan including the full test rig by using Lattice Boltzmann Method. In: Internationl Conference on Fan Noise, Technology and Numerical Methods. Lyon, France, April 15-17, 2015.
5. Magne S, Sanjose M, Moreau S, Berry A, Gerard A. Tonal Noise Control of Centrifugal Fan Using Flow Obstructions - Experimental and Numerical Approaches. In: 19th AIAA/CEAS Aeroacoustics Conference. Berlin, Germany, May 27-29, 2013.
6. Perot F, Kim M-S, Le Goff V, Carniel X, Goth Y, Chassaignon C. Numerical optimization of the tonal noise of a backward centrifugal fan using a flow obstruction. Noise Control Engineering Journal 2013; 61(3):307–19.
7. Bhatnagar PL, Gross EP, Krook M. A Model for Collision Processes in Gases. I. Small Amplitude Processes in Charged and Neutral One-Component Systems. Phys. Rev. 1954; 94(3):511–25.
8. Hänel D. Molekulare Gasdynamik: Einführung in die kinetische Theorie der Gase und Lattice-Boltzmann-Methoden. Berlin, Heidelberg: Springer; 2004.
9. Guo Z, Shu C. Lattice Boltzmann Method and Its Applications in Engineering. New Jersey: World Scientific; 2013. (Advances in computational fluid dynamics).
10. ebm-papst. EC centrifugal fans - RadiCal®: Series R3G190 RD Ø190 mm; 2019 [cited 2019 May 22]. Available from: URL: https://www.ebmpapst.us/media/content/literature/datasheets/R3G190-RD.pdf.
11. Brès G, Pérot F, Freed D. Properties of the Lattice Boltzmann Method for Acoustics. In: 15th AIAA/CEAS Aeroacoustics Conference (30th AIAA Aeroacoustics Conference). Miami, Florida, May 11-13, 2009.